

Galaxy morphology to $I = 25$ mag in the *Hubble Deep Field*

R. G. Abraham¹, N. R. Tanvir¹, B. X. Santiago¹, R. S. Ellis¹, K. Glazebrook²,
& S. van den Bergh³

¹*Institute of Astronomy, University of Cambridge, Madingley Rd. Cambridge CB3 0HA*

²*Anglo-Australian Observatory, P. O. Box 296, Epping, NSW 2121, Australia*

³*Dominion Astrophysical Observatory, National Research Council of Canada, 5071 W. Saanich Rd. Victoria, B. C. V8X 4M6 Canada*

Received: Jan. 31, 1996 Accepted: Feb. 8, 1996

ABSTRACT

The morphological properties of galaxies between $21 \text{ mag} < I < 25 \text{ mag}$ in the *Hubble Deep Field* are investigated using a quantitative classification system based on measurements of the central concentration and asymmetry of galaxian light. The class distribution of objects in the *Hubble Deep Field* is strongly skewed towards highly asymmetric objects, relative to distributions from both the *HST Medium Deep Survey* at $I < 22 \text{ mag}$ and an artificially redshifted sample of local galaxies. The steeply rising number count-magnitude relation for irregular/peculiar/merging systems at $I < 22 \text{ mag}$ reported in Glazebrook *et al.* (1995a) continues to at least $I = 25 \text{ mag}$. Although these peculiar systems are predominantly blue at optical wavelengths, a significant fraction also exhibit red $U - B$ colours, which may indicate they are at high redshift. Beyond Glazebrook *et al.*'s magnitude limit the spiral counts appear to rise more steeply than high-normalization no-evolution predictions, whereas those of elliptical/S0 galaxies only slightly exceed such predictions and may turn-over beyond $I \sim 24 \text{ mag}$. These results are compared with those from previous investigations of faint galaxy morphology with HST and the possible implications are briefly discussed. The large fraction of peculiar/irregular/merging systems in the *Hubble Deep Field* suggests that by $I \sim 25 \text{ mag}$ the conventional Hubble system no longer provides an adequate description of the morphological characteristics of a high fraction of field galaxies.

Key words: Cosmology – Galaxy Evolution – Space Telescope

1 INTRODUCTION

The *Hubble Deep Field* (HDF) is a four square arcminute area of sky at RA 12h 36m 49.4s Dec +62° 12' 58.0" (J2000) observed during December 1995 with the *Hubble Space Telescope* (HST). The images, obtained during 150 orbits with the Wide Field and Planetary Camera 2 (WFPC-2), represent the deepest optical imaging survey yet undertaken (Williams *et al.* 1996). Four broadband filters were used whose wavelength coverage samples the range between the ultraviolet and near infrared (roughly $UBVI$). In the I -band (F814W), the HDF data reaches $\sim 3 \text{ mag}$ fainter than the deepest ground-based observations at similar wavelength (Smail *et al.* 1995), and $\sim 1 \text{ mag}$ fainter than the deepest I -band observations undertaken previously with the HST. The position of the HDF was pre-selected to be a “typical” sample of the high galactic latitude sky in terms of galaxy surface density, while also avoiding bright stars or other objects whose presence might compromise the depth of the observations.

A major objective of the HDF program is to determine

the nature of the rapidly evolving faint blue galaxy population seen in ground-based spectroscopic and photometric surveys conducted over the past decade (Broadhurst, Ellis, & Shanks 1988; Tyson 1988; Colless *et al.* 1990; Ellis 1990; Koo & Kron 1992; Lilly 1993; Tresse *et al.* 1993; Cowie *et al.* 1994; Glazebrook *et al.* 1995b). Many of these objects are distant ($z > 0.3$), and currently only the HST provides the resolution needed to characterise their morphological properties. Results to date have proved difficult to reconcile however, in part perhaps because of the inherently qualitative nature of galaxy classification. Number counts from a sample of 301 galaxies with $I < 22 \text{ mag}$ taken from 13 WFPC-2 fields from the *Medium Deep Survey* (MDS) have been reported by Glazebrook *et al.* (1995a). These authors classified galaxies by eye and found the number-magnitude relationships for elliptical and spiral populations to be consistent with the predictions of high-normalization no-evolution cosmological models, but that the number of irregular/peculiar (possibly merging) galaxies were at least an order of magnitude greater than predicted by the same models. A sim-

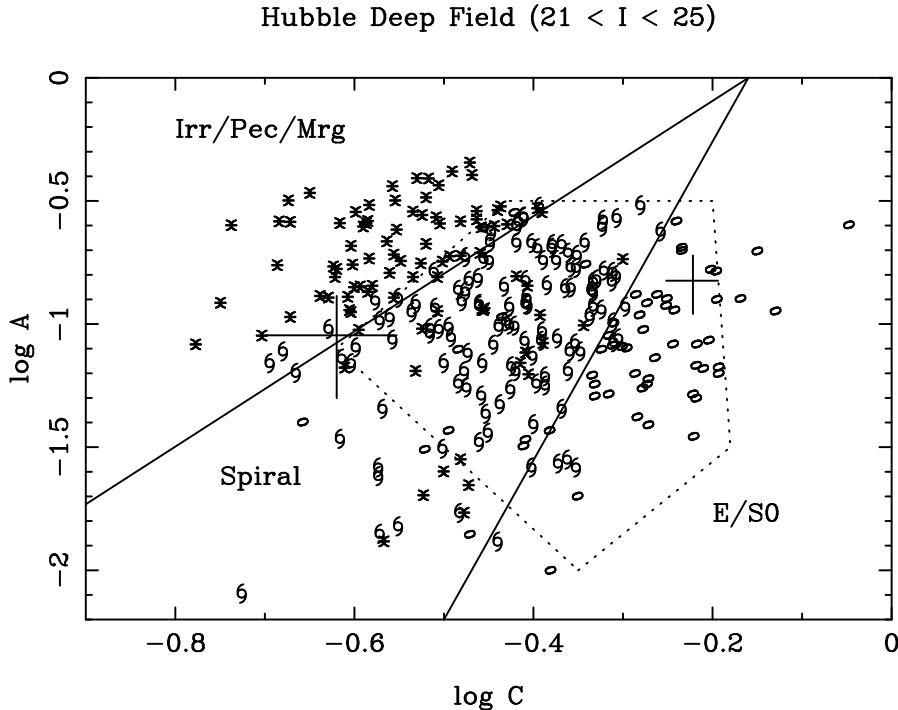


Figure 1. Asymmetry vs. central concentration for galaxies in the Hubble Deep Field. RSE’s visual morphological classifications are keyed to the plot symbols: E/S0’s are shown as ellipses, spirals earlier than Sd are shown as spirals, and irregulars/peculiars/mergers are shown as asterisks. The sectors subdivide the diagram into regions where each of these morphological types dominates. Representative error bars are shown. The dotted polygon shows the “convex hull” enclosing the artificially redshifted local sample of objects described in the text.

ilar conclusion was reached by Driver *et al.* (1995) based on number counts from a single deeper MDS WFPC-2 field to $I=24.25$ mag and by Abraham *et al.* (1996) from automated morphological classification of 521 galaxies from a larger number (21) of WFPC-2 MDS fields to $I=22$ mag.

In contrast, HST observations reported by Schade *et al.* (1995) of a small but spectroscopically complete sample of 32 galaxies from the Canada-France Redshift Survey (CFRS) indicate that the morphological mix at $z \sim 0.75$ is similar to that seen locally, except for a population of “blue nucleated galaxies” (BNGs) which Schade *et al.* suggest comprise $\sim 35\%$ of the faint blue galaxy population. The existence of another major population of morphologically distinct objects, linear “chain galaxies” that may be proto-galactic systems, has recently been reported by Cowie *et al.* (1995) on the basis of HST observations of faint objects ($I > 23$ mag) identified in the Hawaii Deep Survey.

A major advantage of the HDF dataset over the earlier images of Glazebrook *et al.*, Schade *et al.*, Driver *et al.*, and Cowie *et al.* is the improved signal-to-noise level arising from the considerably longer HDF exposure time. The exposure times available to those authors were 5-8 hours in F814W, which is substantially less than the ≈ 35 hours devoted to the HDF in this filter. The improved signal to noise at faint limits enables us to extend the work already begun with the MDS, whose wider spatial coverage nicely complements the HDF data.

Although interesting questions (which the HDF may ultimately answer) concern the very faint ($I > 25$ mag) galaxy

counts, in this short note we are concerned with understanding the morphology and colour distributions of the ~ 300 objects brighter than $I=25$ mag. As described below, at this limit the bulk of the galaxy population is detectable in all four HDF passbands, and morphological classifications are as robust as was the case in our earlier analyses of the MDS data to $I=22$ mag.

A plan of the paper follows. In §2 we review our morphological classification techniques in the context of the HDF data. Section 3 discusses the colour distribution as a function of morphology and, in §4, we combine our dataset with that of the MDS, enabling us to extend Glazebrook *et al.* (1995a)’s morphological galaxy count diagram three magnitudes fainter. A number of new trends appear whose implications are briefly discussed.

2 MORPHOLOGICAL ANALYSIS OF THE HUBBLE DEEP FIELD

Working with the “dithered” (resampled by a factor of 2.5 and stacked) version 1 HDF images released by STScI, we constructed a source catalog using the APM faint-object photometry software (Irwin 1985). At very faint ($I \gtrsim 27$ mag) levels, the number of objects in the resulting catalog depends sensitively on the smoothing scale, detection threshold, and minimum object area used by the software, but in the regime where morphological classification is reliable ($I < 25$ mag) the final catalog is robust. The

photometry was calibrated on the instrumental magnitude system defined by Holtzmann *et al.* (1995). Glazebrook *et al.* (1995a) used the same *I*-band calibration in their MDS analysis and thus the results are directly comparable. The structural properties of galaxies on the *I*-band frame in the magnitude range $21 \text{ mag} < I < 25 \text{ mag}$ were investigated with the automated morphological analysis system used by Abraham *et al.* (1996) to characterise objects from the MDS. Visual classifications were also made by two of us (RSE and vdB) using the classification system discussed by Glazebrook *et al.* (1995a). The reader is referred to these earlier papers, and to Abraham *et al.* (1994), for further details of these procedures beyond the outline given here.

In the automated classification procedure, the galaxy images were first isolated from the sky background by extracting contiguous pixels at least 1σ above the sky level. For each galaxy an asymmetry index, A , was measured by rotating and self-subtracting the galaxy image from itself. A second parameter in the classification procedure, central concentration C , is determined from measurements of the intensity-weighted second order moments of the galaxy images. Asymmetric or disturbed galaxies generally have high values of A and low values of C , ordinary spirals have intermediate values of both parameters, and early-types are distinguished by high central concentration.

In order to compare directly the measurements of C and A obtained from “dithered” HDF images to those obtained from the MDS, the 23 galaxies in the HDF with $21 \text{ mag} < I < 22 \text{ mag}$ (the magnitude limit of the Medium Deep Survey) were rebinned to the original sampling of the WFPC-2 camera and degraded by adding Poisson noise to simulate the appearance of these objects under typical (~ 5000 s) MDS exposures. A comparison of measurements from the original and degraded images indicated that the HDF dithering procedure introduces a small systematic change in the measured asymmetry value of the HDF data, $\Delta A = 0.053 \pm 0.02$, relative to undithered MDS data. This small offset was therefore subtracted from the measured asymmetry values when comparing the HDF and MDS. It is emphasized that applying this correction *decreases* the total number of asymmetric objects in the HDF. Random errors were determined by Monte Carlo simulation (c.f. Abraham *et al.* 1994 and 1996) and are no larger than $\Delta C = \Delta A = 0.07$ to $I=25 \text{ mag}$. Both C and A depend on the rest frame isophote level at which the measurements are made. The 1σ limiting isophote of the HDF data ($\sim 26.5 \text{ mag arcsec}^{-2}$) is $1.5 - 2 \text{ mag arcsec}^{-2}$ deeper than the corresponding limiting isophote for more typical HST data (e.g. from the MDS), so bright galaxies in the HDF are probed to larger radii than corresponding objects in the MDS. Strong $(1+z)^4$ cosmological dimming is expected to roughly synchronize the rest-frame limiting isophotes for the MDS and HDF samples at faint magnitudes, but a detailed assessment of this effect must await redshift information (discussed below).

The distribution of HDF galaxies in the $\log(A)$ vs. $\log(C)$ plane is shown in Figure 1. The visual classifications of RSE are indicated by the plot symbols on this Figure, and are in excellent agreement with classifications based on position on the $\log(A)$ vs. $\log(C)$ diagram. Using the visual classifications and the simulations described below, three sectors were defined on the diagram, subdividing the galaxy pop-

ulation into irregular/peculiar/mergers, spirals, and E/S0 systems (the same bins adopted by Glazebrook *et al.* 1995a, and Abraham *et al.* 1996). The HDF asymmetry values are skewed markedly towards highly asymmetric galaxies relative to the MDS, as shown in Figure 2. (Note that Abraham *et al.* 1996 argue that the MDS data is itself skewed to high asymmetry with respect to local samples.) Because the HDF galaxies are presumably at higher redshifts than their MDS counterparts, it is important to consider whether this shift may arise from bandshifting or k -correction biases, *i.e.* whether the differences are simply a result of our observing ever further into the rest-frame ultraviolet for more distant galaxies.

Only limited constraints are currently available for the redshift distribution of field galaxies to the faint limits explored in this paper. Using arguments based on the gravitational lensing signal in well-constrained clusters, Smail *et al.* (1994) and Kneib *et al.* (1996) claim that most objects will lie in the range $0.5 < z < 2.5$. In order to determine the importance of bandshifting effects on galaxies at these redshifts, C and A were measured for Frei *et al.* (1995)’s sample of “generic” Hubble types between $T = -5$ (ellipticals) and $T = 6$ (Scd galaxies) after artificially redshifting them to $z = 0.5, 1.0, 1.5,$ and 2.0 . As described in Abraham *et al.* (1996), k -corrections were applied to each image using the observed colour at each position on the galaxy to interpolate between a set of template non-evolving SEDs (kindly supplied by A. Aragón-Salamanca). The artificially redshifted galaxies occupied the region of the $\log(A)$ vs. $\log(C)$ diagram within the dotted polygon shown in Figure 1, which therefore maps out the portion of this diagram which is expected to be occupied by distant *non-evolving* galaxies with Hubble T -types between -5 and 6 . It appears that the majority of objects in the peculiar/irregular/merger sector of Figure 1 correspond to one or more of the following: (a) to Hubble types later than Sd, (b) to significantly evolved intermediate Hubble-type spirals, or (c) to a family of objects outside the Hubble system (*i.e.* merging or peculiar galaxies).

At this point we introduce the visual classifications made for the sample by RSE and vdB. These classifications are in good agreement with classifications from the $A - C$ scheme on a one-to-one basis and reproduce well the boundaries of the classes identified from the simulations discussed above (Figure 1). Agreement was particularly good for the spheroidal systems and, where differences between visual and machine classifications were found, they generally lay at the boundaries of the 3 categories. Both vdB and RSE noted that beyond $I \gtrsim 24 \text{ mag}$ an increasing proportion of faintest spheroidal and spiral galaxies were less regular than brighter examples, and, in particular, there was a notable absence of “grand-design” spirals. Asymmetries in galaxies often resulted from one or more off-centred knots of activity, suggestive of either increased star-formation or ultraviolet signal in very distant sources (and emphasizing the importance of accounting for bandshifting effects). A montage of typical galaxies with $I > 23 \text{ mag}$ is given in Figure 3 [Plate 1].

Although some of the irregular galaxies in the HDF appear spectacularly “chain-like”, the surface density of strictly linear systems with multiple knots and narrow transverse extents to $I = 25 \text{ mag}$ is $\lesssim 2.5 \text{ arcmin}^{-2}$, *i.e.* a relatively small fraction of the total number of irregulars.

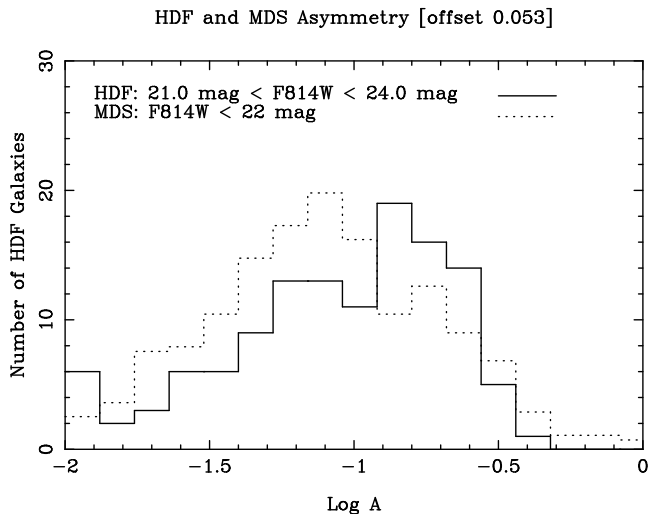


Figure 2. Histograms of the asymmetry parameter, A , for galaxies in the Hubble Deep Field (solid line) and Medium Deep Survey (dashed line). Note the marked skewness of the HDF data towards asymmetric galaxies. The MDS histogram has been normalized to match approximately the total counts in the HDF. The mean asymmetry of the HDF histogram has been reduced slightly (as described in the text) to correct for the effects of dithering in the images.

Figure 3. (Plate 1). Montage of $I > 23$ galaxies from the HDF with: Irr/Pec/Mrg – columns 1 and 2; Spirals – columns 3 and 4; and E/S0 – columns 5 and 6. Images were selected on the basis of the $A-C$ classifier (see Figure 1).

There are a larger number of objects which have a bright nucleus and a faint, one-sided tail, and the properties of these “tadpole-like” galaxies (which are possibly related to the chain-like systems), will be described in a future work (van den Bergh *et al.*, in preparation).

3 COLOURS

A very significant advantage of the HDF over earlier data is the extensive imaging conducted in F300W (hereafter U), F450W (B) and F606W (V). In the following we will use instrumental magnitudes for the UBV system since our discussion is only based on relative colours. The $I=25$ mag limit for the present investigation not only corresponds to that point where sound morphological classifications can be determined (§2) but also to that limit at which most of the galaxies are reliably detected in all 4 bands; the U band is the shallowest exposure and is essentially complete (3σ) at $U \simeq 27$. Thus, only a few very red objects ($U - I > 2$) in our $I < 25$ sample are undetected in U .

Figure 4 [Plate 2] presents the $U - B$ (F300W – F450W), $B - V$ (F450W – F606W), $V - I$ (F606W – F814W), and $B - I$ (F450W – F814W) colours, obtained through 0.4 arc-sec apertures, for the HDF sample as a function of position on the morphological $\log(A)$ vs. $\log(C)$ diagram. The colour of an individual galaxy is represented by the colour of the corresponding symbol on this plot. The trend from one set

Figure 4. (Plate 2). The $U - B$ (top left), $B - V$ (top right), $V - I$ (bottom left), and $B - I$ (bottom right) colours for the HDF sample as a function of position on the morphological $\log(A)$ vs. $\log(C)$ diagram. Symbols indicate each object’s colour. Positions on the morphological diagram are based upon I -band morphology. Sectors that subdivide approximately the “peculiar/irregular/merger”, “spiral”, and “early-type” portions of the diagram (defined as for Figure 1) are shown by solid lines. Note the strong correlation between optical colour and morphology. Most peculiar systems are optically blue, but many of these galaxies also exhibit red $U - B$ colours.

of passband colours to the next is remarkably similar. The dominant colour axis appears horizontal, as expected from the close correspondence between central concentration and bulge-to-disk ratio (Abraham *et al.* 1994). The “faint blue galaxies” determined from optical colours correspond to low-central concentration, highly asymmetric objects as originally claimed by Glazebrook *et al.* (1995a). Objects classified as early-types are predominantly red, indirectly supporting the accuracy of classifications made on the basis of C and A , and in agreement with observations suggesting that the early-type population in the field remains old even at faint flux levels.

The distribution of irregular/peculiar/merger objects on the $U - B$ diagram exhibits an interesting behaviour (shown more clearly in Figure 5). Nineteen of 83 objects in this morphological category (determined from Figure 1) have *blue* optical-near infrared colours ($V - I < 0.6$) and comparatively *red* UV-optical colours ($U - B > -0.2$). In fact, objects which are red in $U - B$ tend to have high asymmetry irrespective of morphological class - a trend which is not present in other colours. They are also faint, with only two of the “ $U - B$ red, $V - I$ blue” objects being brighter than $I = 23$ mag. One possibility is that a significant fraction of asymmetric objects have $z > 2.3$ corresponding to the Lyman discontinuity entering the U filter. Alternatively this may be the result of reddening from dust catalysed by mergers or interactions; this seems less likely as it would produce a trend in the other colours.

4 NUMBER COUNTS

The high signal-to-noise ratio of the HDF data and the reliability of the morphological classifications allow us to extend the morphologically segregated galaxy counts 3 magnitudes deeper than was possible with the Medium Deep Survey. This dramatic improvement reflects the fact that signal-to-noise is the prime limitation in image analysis; the increase in angular diameter distance corresponding to the 3 magnitude improvement is probably very small. Figure 6 combines the HDF and MDS number counts (with error bars based on Poisson statistics). Also shown are the no-evolution predictions for each type constructed as described in Glazebrook *et al.* (1995a), adopting Schechter luminosity functions (LFs) with parameters given by Loveday *et al.* (1992), and a high normalization ($\phi_* = 0.03h^3 \text{ Mpc}^{-3}$). The elliptical panel shows the predicted counts resulting from a flat faint-end slope ($\alpha = -1$), instead of Loveday’s original steep faint-end slope. The very small difference between the counts determined using the $A - C$ classifications and those

Colour-Colour Diagram Highlighting Low C/High A Objects

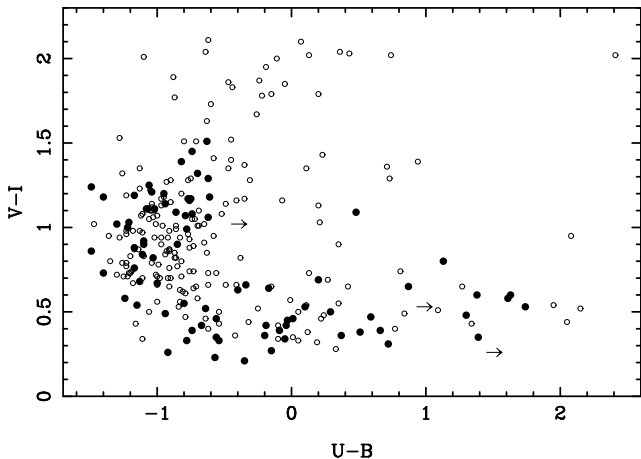


Figure 5. The $V - I$ vs $U - B$ colour-colour diagram for all objects with $I < 25$ mag. Bold symbols denote objects in the irregular/peculiar/merger sector of Figure 1. The small number of objects with no $U - B$ colour are represented by lower limits. Note the plume of objects with blue $V - I$ and red $U - B$ colours.

determined visually by RSE and vdB are also indicated in the Figure.

The HDF counts extend the trend already identified by Glazebrook *et al.* (1995a) to much fainter magnitudes. The over-abundance of irregular/peculiar/merging systems continues to the $I = 25$ mag limit, at which point these systems represent over 40% of all galaxies. As discussed above, a significant fraction of these systems may lie beyond a redshift $z \simeq 2.5$ and there appears to be a general evolution of increasing asymmetry with redshift. Significantly, some new trends emerge from Figure 6. Beyond $I = 22$ mag the spiral counts now show a significant excess over the no-evolution predictions. A weaker trend is seen for the spheroidal systems (whose counts are only marginally above the no-evolution prediction) and there is some evidence of a turn-over in the last magnitude interval.

The interpretation of Figure 6 depends crucially on both the redshift distribution of the data and the faint end slope of the luminosity function. If the local luminosity function is reliably determined from recent faint surveys (c.f. Ellis *et al.* 1996) and the Lyman limit is always present in distant galaxies, the spiral excess would appear to imply luminosity evolution for disk galaxies in the interval $1 < z < 2.5$. The flattening of the spheroidal galaxy counts beyond $I = 24$ mag in both the visual and automated catalogues is an interesting, though currently uncertain, result. As this population is predominantly red, minimal evolution is implied to quite high redshift and steepening α would make this result yet tighter. The effect of curvature here is slight: in the absence of luminosity evolution, the bulk of the $I \simeq 24-25$ spheroidals are expected to lie within $z < 2$. In this respect, the decline in the counts is a puzzling result although it may indicate that the precursors of many present-day spheroidals lie in one of the other morphological categories.

The large fraction of irregular/peculiar/merger systems detected at faint magnitudes in the HDF supports earlier

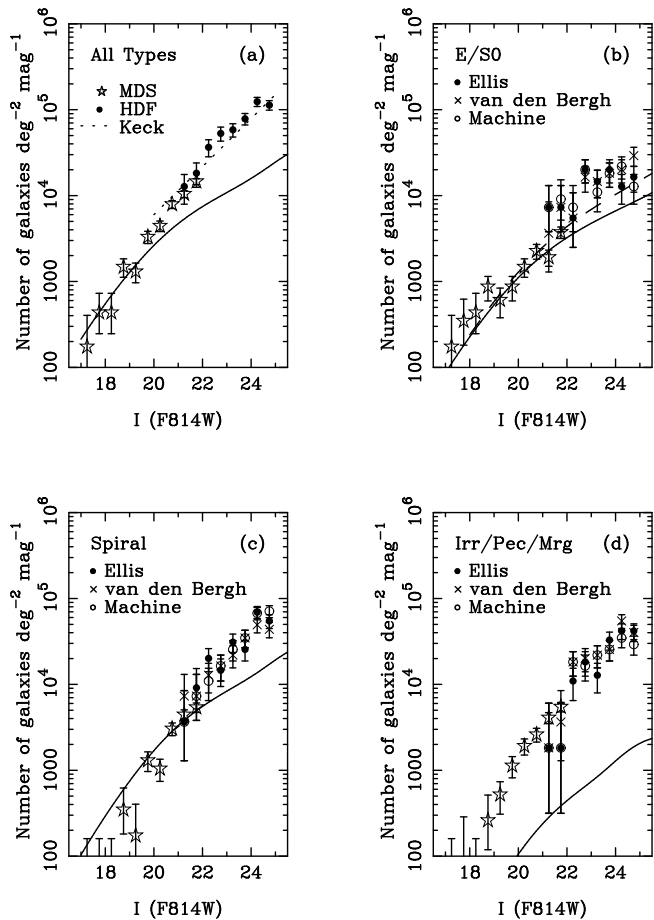


Figure 6. The number-magnitude relations for morphologically segregated samples of galaxies from the HDF and MDS. Open circles indicate counts obtained from automated classifications determined from Figure 1, closed circles indicate the results from the visual classifications of RSE, and crosses indicate the results from the visual classifications of vdB. The MDS counts are indicated by the stars on each panel. The no-evolution $\Omega = 1$ curves from Glazebrook *et al.* (1995a), extrapolated to $I = 25$ mag, are superposed. The dashed line on the E/S0 diagram shows the effect of assuming $\Omega = 0.1$. The dotted line in panel (a) shows the I -band number counts determined by Smail *et al.* (1995) from two deep fields imaged with the Keck telescope.

suggestions that beyond $I \sim 24$ mag the conventional Hubble system no longer provides an adequate description of the structural characteristics for a significant fraction of galactic (and possibly proto-galactic) systems. This has important implications for forthcoming number count and correlation analyses of the *Hubble Deep Field*. The results from fainter investigations may depend strongly on the prescription used to define galaxies amongst collections of clumpy subcomponents. Although the magnitude limit in this paper was chosen deliberately so as to minimise this ambiguity, the peculiar structure and obvious distortion of conventional galactic features seen in many systems at $I < 25$ mag inevitably results in some difficulties when trying to connect these objects to local counterparts. At $I < 25$ mag it still seems useful to exploit the (approximate) connection between sectors on

the $A - C$ diagram and conventional galaxy classifications in order to determine number counts that can be directly compared with those for the Hubble system. But for fainter galaxies it may prove more useful to model the distributions of C and A (or other structural parameters) directly, and no longer require galaxies to be directly mapped onto bins corresponding to local archetypes. A quantitative characterisation of the morphologies of faint galaxies, based on measurements of physically meaningful structural parameters, provides an objective route forward when the conventional “syntax” of morphological description, based on the Hubble system and references to local archetypes, has broken down.

ACKNOWLEDGMENTS

We thank Bob Williams for devoting such a large fraction of Director’s Discretionary Time to the HDF project, and are grateful to the staff of STScI and ST-ECF for mobilising in order to ensure that the HDF data was reduced and available quickly. We also thank the UK HST Support Facility for help in obtaining the HDF data, Daniel Durand of the Canadian Astronomy Data Centre for help with displaying the images at DAO, and the members (and former members) of the Cambridge APM group, especially Steve Maddox and Mike Irwin, for useful discussions with regard to catalog construction with the APM software.

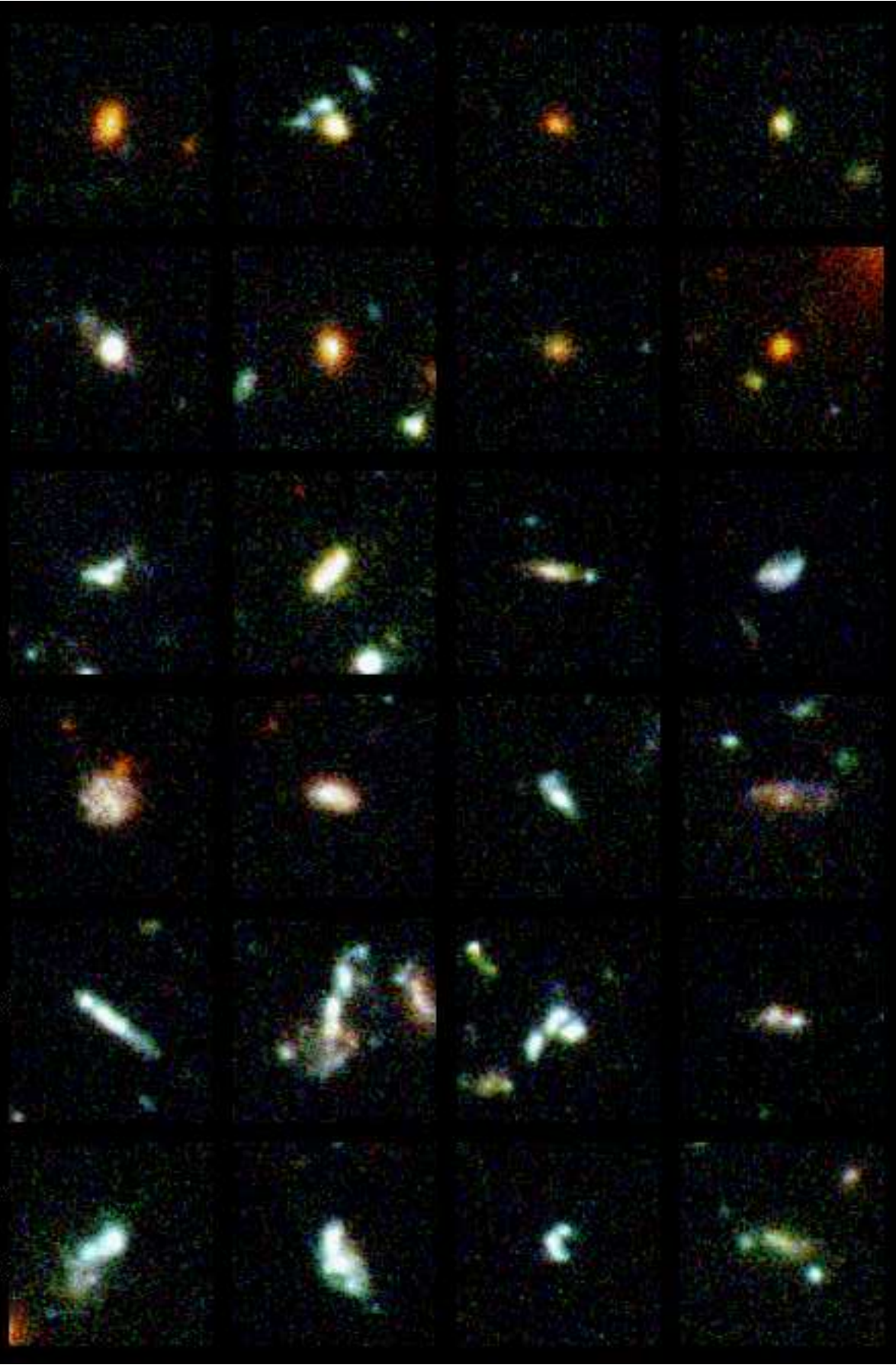
REFERENCES

- Abraham, R.G., Valdes, F., Yee, H.K.C. & van den Bergh, S. 1994, *ApJ*, 432, 75
- Abraham, R.G., van den Bergh, S., Glazebrook, K., Ellis, R.S., Santiago, B. X., Surma, P., & Griffiths, R. 1996, *ApJ* (submitted).
- Broadhurst, T., Ellis, R., & Shanks, T. 1988, *MNRAS*, 235, 827
- Colless M., Ellis R. S., Taylor, K., Hook, R. N. 1990, *MNRAS*, 244, 408
- Cowie, L. L., Gardner, J. P., Hu, E. M., Songaila, A., Hodapp, K. W., Wainscoat, R. J. 1994 *ApJSupp*, 94, 461
- Cowie, L. L., Hu, E. M., & Songaila, A. J., *ApJ* (In Press).
- Dressler, A., Oemler, A., Butcher, H. R., and Gunn, J. E. 1994, *ApJ*, 430, 107–120.
- Driver, S.P., Windhorst, R.A. & Griffiths, R.E. 1995, *ApJ*, 453, 48.
- Ellis, R. S. 1990, in Kron R. G., ed., *ASP Conf. Ser. Vol 10, Evolution of the Universe of Galaxies*. Astron. Soc. Pac., San Francisco, p. 248
- Ellis, R.S., Colless, M., Broadhurst, T.J., Heyl, J.S. & Glazebrook, K., *MNRAS*, in press.
- Glazebrook, K., Ellis, R., Santiago, B. & Griffiths, R. 1995a, *MNRAS*, 175, L19.
- Glazebrook, K., Ellis, R. S., Colless, M. M., Broadhurst, T. J., Allington-Smith, J. R., & Tanvir, N. R. 1995b, *MNRAS*, 273, 157
- Griffiths, R.F. *et al.* 1994, *ApJ*, 437, 67.
- Holtzmann, J.A., *et al.* 1995, *PASP*, 107, 1065.
- Irwin, M.J. 1985, *MNRAS*, 214, 575.
- Koo, D. C., & Kron, R. 1992, *Ann. Rev.* 30, 613.
- Kneib, J-P, Ellis, R.S., Smail, I.R., Couch, W.J. & Sharples, R.M., *ApJ* submitted.
- Lilly, S. J. 1993, *ApJ*, 411, 401
- Loveday, J., Peterson, B. A., Efstathiou, G., Maddox, S. J. 1992, *ApJ*, 390, 338
- Schade, D., Lilly, S.J., Crampton, D., Hammer, F., Le Fèvre, O. & Tresse, L., *ApJLett* (in press).
- Smail, I., Ellis, R.S. & Fitchett, M.J., *MNRAS*, 270, 245.
- Smail, I., Hogg, D. W., Yan, L., & Cohen, J., *ApJ*, 449, 105.
- Tresse, L., Hammer, F., Le Fèvre, O., Proust, D. 1993, *A&A*, 277, 53
- Tyson, J. A. 1988, *AJ*, 96, 1
- Williams, R.E. *et al.* 1996, *Science with the Hubble Space Telescope - II*, eds, Benvenuti, P., Macchetto, F.D., Schreier, E.J., STScI, in press

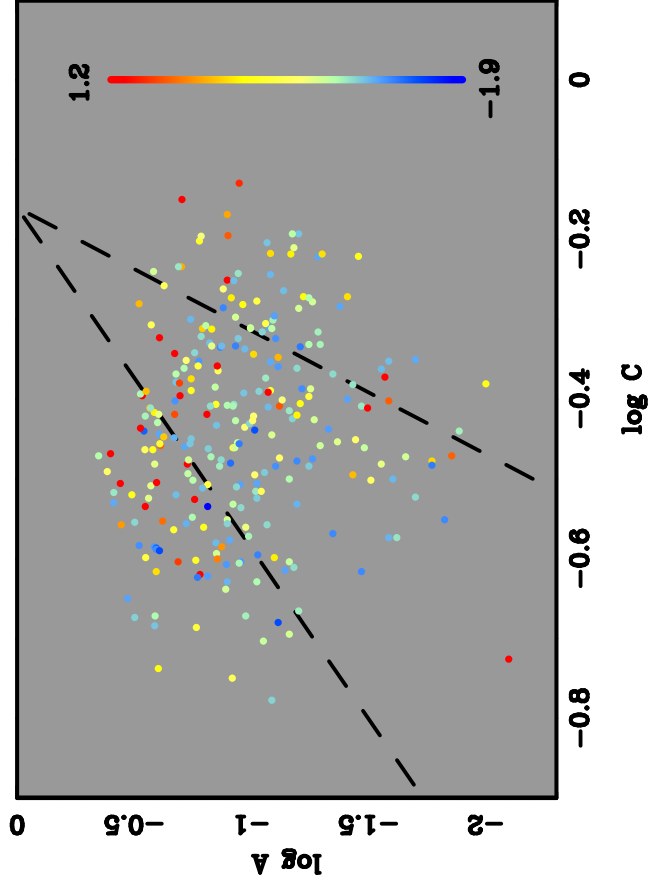
Irregular/peculiar/merger

Spiral

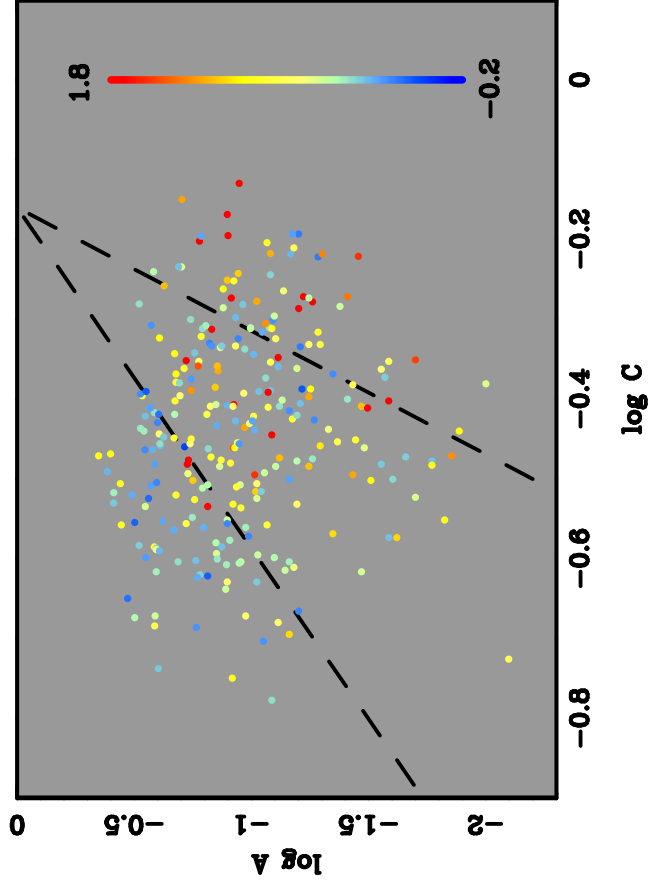
Elliptical/S0



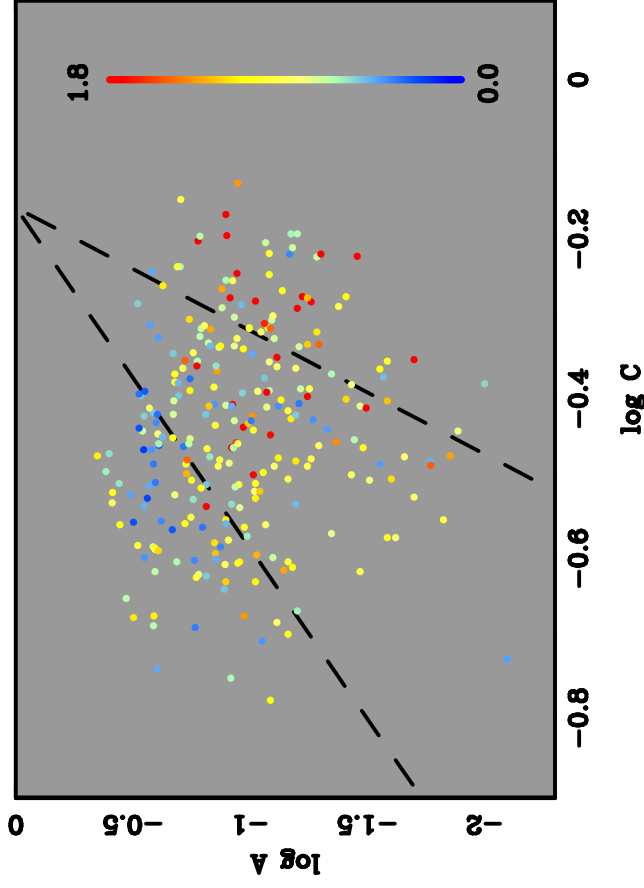
Hubble Deep Field ($21 < I < 25$) U-B Colors



Hubble Deep Field ($21 < I < 25$) B-V Colors



Hubble Deep Field ($21 < I < 25$) V-I Colors



Hubble Deep Field ($21 < I < 25$) B-I Colors

